Journal of Advances in Applied Mathematics, Vol. 6, No. 3, July 2021
https://dx.doi.org/10.22606/jaam.2021.63002

Predictive Continuum Constitutive Modeling of Unfilled and Filled Rubbers

Fuzhang Zhao

APD Optima Study, Lake Forest, CA 92630, USA
Email: fuzhangzhao@yahoo.com

Abstract The general CSE model fits Treloar's uniaxial extension test and predicts unfitted uniaxial compression, equibiaxial extension, biaxial extension, pure shear, and simple shear tests. As a newly proposed method, the general CSE model, along with the stress-softening ratio, the residual-stretch ratio, and the weighted piecewise two-point interpolation function, fits the Cheng–Chen's test and the Diani–Fayolle–Gilormini's test in cyclic uniaxial extension at different pre-stretches and predicts corresponding responses at untested pre-stretches. Physical mechanisms of the Mullins effect have also been predicted based on the evolution of constitutive parameters.

Keywords: Filled rubber, general CSE functional, Mullins effect, predictive constitutive modeling, unfilled rubber.

Nomenclature

$\mathbf{C}$	right Cauchy–Green tensor
c_1, c_2, c_3, c_4	constitutive parameters
$\mathbf{E}$	Green–Lagrange strain tensor
$\mathbf{F}, \mathbf{F}_e, \mathbf{F}_p$	total, elastic, plastic deformation gradient tensors
f, g, h	three arbitrary functions
$\mathbf{I}$	second-order unit tensor
I_1, I_2, I_3	invariants of the right Cauchy–Green tensor
i, j, n	two indexes for three orthogonal directions, nth cycle
P, P_0, P_n	nominal stresses in general, virgin, nth cycle
P_{be1}, P_{be2}, P_{ee}	nominal stresses in biaxial extension, equibiaxial extension
P_{ij}	nominal stress tensor in indicial notation
P_{ps}, P_{ss}	nominal stresses in pure shear, simple shear
P_{uc}, P_{ue}	nominal stresses in uniaxial compression, uniaxial extension
P_{ur}	nominal stress in uniaxial extension with residual stretch
R_{rn}, R_{sn}	residual-stretch ratio, stress-softening ratio in nth cycle
r_1	parameter for residual-stretch ratio function
$\mathbf{S}$	second Piola–Kirchhoff stress tensor
s_1, s_2	parameters for stress-softening ratio function
w	weight for the piecewise two-point interpolation function
Greek Symbols	
κ	shear stretch
Λ, λ	ratio of total stretch to residual stretch, normal stretch
$\Lambda_p, \Lambda_{p1}, \Lambda_{p2}$	normalized untested pre-stretch and tested pre-stretches
$\lambda_r, \lambda_{r0}, \lambda_{rn}$	residual stretches in general, virgin, nth cycle
$\Psi, \Psi_{\mathbf{E}}$	isotropic CSE functional or model, its covariant functional
ψ_1, ψ_2, ψ_3	three independent first-integrals used in Lie group method
Abbreviations	
CSE	continuum stored energy
LLSQ	linear least squares
EPDM	ethylene-propylene-diene monomer
NR-S8	natural rubber vulcanized with 8 phr sulfur
SBR	styrene-butadiene rubber
TED	trial-and-error-on-digit

1 Introduction

Natural rubbers and synthetic elastomers with a wide range of applications, including but not limited to tires, engine mounts, seals, dampers, hoses, tunnel linings, and bump stoppers, can be classified as isotropic hyperelastic materials. Sulfur vulcanization and filler reinforcements are fundamental manufacturing processes for achieving desired properties of rubber materials and performances of rubber products. Sulfur vulcanization is a chemical process that converts natural rubbers and synthetic elastomers into crosslinked rubbers and elastomers. Fillers such as carbon-black, silica, and other nano-structured particles are usually added during reinforcement processes, in which filled rubbers have enhanced material properties such as abrasion resistance, tear strength, tensile strength, wear, and fatigue. The mechanical responses of elastomeric materials under cyclic loading exhibit stress-softening, hysteresis loop, permanent stretch set, permanent stress set, anisotropy, and loading rate effects. The stress-softening induced from previous stretches has generally become known as the Mullins effect [1]. Both unfilled and filled rubbers exhibit the Mullins effect, which is more pronounced for filled rubbers. Stress-softening of filled vulcanizates mainly occurs at the first stretch, gradually reduces at stretches less than the previous stretch, but changes relatively little at ever higher stretches and after several cycles of reloading and unloading. Failure of components made of carbon-black filled rubbers has drawn attention to the need for a better understanding of the physical mechanisms of the Mullins effect and the possible causes of a failure [2]. With appropriate experimental characterizations, predictive constitutive models, and actual microscopic observations, physical mechanisms of the Mullins effect can be better understood.

The two-phase model, with soft matrix and hard filler phases, was postulated by Mullins and Tobin [3]. Two-phase models have been further developed by Wineman and Rajagopal [4], Wineman and Huntley [5], Johnson and Beatty [6], Beatty and Krishnaswamy [7], Zúñiga and Beatty [8], Qi and Boyce [9], and others. Models based on continuum damage mechanics, with a statistical mechanics approach, have been developed to simulate the Mullins effect by Gurtin and Francis [10], Simo [11], Govindjee and Simo [12,13], De Souza Neto, Peric, and Owen [14], Miehe [15], Miehe and Keck [16], and many others. The tube model has been applied by Klüppel and Schramm [17], by Lorenz and Klüppel [18], by Raghunath, Juhre, and Klüppel [19], and by Plagge and Klüppel [20]. The network decomposition model has been developed and extended by Dargazany and Itskov [21,22], by Dargazany, Khiêm, and Itskov [23], and by Khiêm and Itskov [24,25]. The pseudo-elastic model was developed by Ogden and Roxburgh [26], Dorfmann and Ogden [27,2], Rickaby and Scott [28], and Naumann and Ihlemannthe [29]. Many models developed include the network alteration theory by Septanika and Ernst [30], extensively applied by Marckmann *et al.* [31], Diani, Brieu, and Vacherand [32], Zhao [33], Wang and Gao [34], and Zhu and Zhong [35,36], the internal sliding and friction thermodynamics model by Cantournet, Desmorat, and Besson [37], and so forth.

Constitutive models and physical mechanisms including bond rupture, molecules slipping, filler rupture, disentanglement, and double-layer for the Mullins effect have been reviewed by Mullins in 1969 [38] and further reviewed by Diani, Fayolle, and Gilormini in 2009 [39]. Physical mechanisms of the Mullins effect have been classified into three categories: damage within the rubber matrix, filler network alteration, and rubber-filler interface change by Diaz, Diani, and Gilormini [40]. Polymer network, filler network, polymer-filler interaction, hydrodynamic amplification, breakdown of filler network are thought to be the key factors for the Mullins effect and the related studies based on statistical mechanics, along with the tube model, have been reviewed by Vilgis, Heinrich, and Klüppel in 2009 [41]. No unanimous agreement has been reached for the physical mechanisms of the Mullins effect. Not many constitutive models can accurately fit uniaxial extension test and predict experimental tests in other deformation modes for both unfilled and filled rubbers. Thus, predictive constitutive modeling and physical understanding of the Mullins effect remains a major challenge despite its extensive studies for more than seven decades.

The major objectives are threefold: (i) to apply the general CSE functional for predictive constitutive modeling of Treloar's tests for an unfilled rubber, (ii) to apply the general CSE functional, the stress-softening ratio, the residual-stretch ratio, and the weighted piecewise two-point interpolation function together as a newly proposed method for predictive constitutive modeling of the Cheng–Chen's test and the Diani–Fayolle–Gilormini's test in cyclic uniaxial extension for filled rubbers with the Mullins effect, and (iii) to predict physical mechanisms of the Mullins effect based on the evolution of constitutive parameters as a function of pre-stretches.

2 Constitutive Modeling of Rubberlike Materials

2.1 General CSE Model

Mathematical models of natural laws are frequently formulated through the concept of symmetry into nonlinear partial differential equations. For constitutive modeling of rubberlike materials with finite isotropic deformations, the second Piola–Kirchhoff stress tensor, $\mathbf{S}$, has been derived in continuum mechanics from the Clausius–Duhem form of the second law of thermodynamics as

$$\mathbf{S} = 2\frac{\partial \Psi}{\partial \mathbf{C}}. \tag{1}$$

An isotropic stored energy functional as function of three invariants of the right Cauchy–Green tensor, $\Psi = \Psi(I_1, I_2, I_3)$, was established by the classical work of Rivlin [42]. Taking derivatives with the chain rule, the general constitutive equation reads

$$\mathbf{S} = 2\left[\left(\frac{\partial \Psi}{\partial I_1} + I_1\frac{\partial \Psi}{\partial I_2}\right)\mathbf{I} - \frac{\partial \Psi}{\partial I_2}\mathbf{C} + I_3\frac{\partial \Psi}{\partial I_3}\mathbf{C}^{-1}\right], \tag{2}$$

where the three invariants of right Cauchy–Green tensor $\mathbf{C}$, I_1, I_2, and I_3, are defined by

$$I_1 = \mathrm{tr}\mathbf{C}, \quad I_2 = \frac{1}{2}\left[(\mathrm{tr}\mathbf{C})^2 - \mathrm{tr}\mathbf{C}^2\right], \quad I_3 = \det\mathbf{C}. \tag{3}$$

For a physically consistent, mathematically covariant, and geometrically meaningful formulation, the CSE functional was postulated and balanced with its stress work done by Zhao [43]

$$\Psi = \mathbf{S} : \frac{\mathbf{C}}{2}. \tag{4}$$

The general CSE functional (4) is covariant to $\Psi_{\mathbf{E}} = \mathbf{S} : \mathbf{E}$ under the transformation of $\mathbf{E} = 0.5(\mathbf{C} - \mathbf{I})$. Substituting (2) into (4), simplifying, and rearranging yields the partial differential equation of the isotropic CSE functional in terms of three symmetric functions I_1, I_2, and I_3

$$\Psi = I_1\frac{\partial \Psi}{\partial I_1} + 2I_2\frac{\partial \Psi}{\partial I_2} + 3I_3\frac{\partial \Psi}{\partial I_3}. \tag{5}$$

With Lie group methods, the characteristic system of (5) takes the form of

$$\frac{\mathrm{d}I_1}{I_1} = \frac{\mathrm{d}I_2}{2I_2} = \frac{\mathrm{d}I_3}{3I_3} = \frac{\mathrm{d}\Psi}{\Psi}. \tag{6}$$

Taking its independent first-integrals, $\psi_1 = I_2/I_1^2$, $\psi_2 = I_3/I_1^3$, and $\psi_3 = \Psi/I_1$, the general solution to the CSE partial differential equation (5) has been obtained as

$$\Psi = I_1 h(I_2/I_1^2, I_3/I_1^3), \tag{7}$$

where h as an arbitrary function has been selected as the summation of two arbitrary functions of invariant groups albeit other available combinations

$$\Psi = I_1\left[f(I_2/I_1^2) + g(I_3/I_1^3)\right], \tag{8}$$

where f and g as two arbitrary functions can be fixed by curvatures of deformations. For normal and shear deformations, the first arbitrary function, f, has been defined as

$$f(I_2/I_1^2) = c_1 + c_2\sqrt{I_2/I_1^2} = c_1 + c_2\frac{\sqrt{I_2}}{I_1}, \tag{9}$$

and for different degrees of ellipsoidal deformations, the second arbitrary function, g, has been generalized and selected as

$$g(I_3/I_1^3) = c_3(I_3/I_1^3)^{-c_4} = c_3\frac{I_1^{3c_4}}{I_3^{c_4}}. \tag{10}$$

For better predictive constitutive modeling mechanical responses of rubbers under monotonic and cyclic loadings, substituting (9) and (10) into (8) yields the general CSE functional [44]. Applying the normalization condition, $\Psi(\mathbf{I}) = 0$, gives

$$\Psi = c_1 (I_1 - 3) + c_2 \left(\sqrt{I_2} - \sqrt{3}\right) + c_3 \left(\frac{I_1^{3c_4+1}}{I_3^{c_4}} - 3^{3c_4+1}\right), \tag{11}$$

where the four constitutive parameters, c_1, c_2, c_3, and c_4, will then be determined by experimental tests. Thus, the general CSE functional will be used to establish constitutive equations of commonly used deformation modes in experimental tests.

2.2 General CSE Constitutive Equations

Nominal stress and stretch results are preferably calculated from force and extension measurements with original sample dimensions recorded in experimental tests. The nominal stress as a function of stretch in indicial notation is generally expressed as

$$P_{ji} = \frac{\partial \Psi}{\partial I_1}\frac{\partial I_1}{\partial \lambda_{ij}} + \frac{\partial \Psi}{\partial I_2}\frac{\partial I_2}{\partial \lambda_{ij}} + \frac{\partial \Psi}{\partial I_3}\frac{\partial I_3}{\partial \lambda_{ij}}, \quad (i, j = 1, 2, 3). \tag{12}$$

The three derivatives of the general CSE functional (11) for rubber-like materials with the incompressible assumption of $I_3 = 1$ are

$$\frac{\partial \Psi}{\partial I_1} = c_1 + c_3(3c_4 + 1)I_1^{3c_4}, \quad \frac{\partial \Psi}{\partial I_2} = \frac{c_2}{2\sqrt{I_2}}, \quad \frac{\partial \Psi}{\partial I_3} = 0. \tag{13}$$

Mechanical characterizations of isotropic hyperelastic materials are often conducted by uniaxial extension, uniaxial compression, equibiaxial extension, biaxial extension, pure shear, and simple shear tests. Thus, the general isotropic CSE constitutive equations in the six testing modes will be derived based on the equations (11) through (13).

Uniaxial Extension and Compression Modes. The nominal stress as a function of principal stretch in uniaxial extension and uniaxial compression modes for incompressible isotropic hyperelastic materials can be unified as

$$P_{ue} = P_{uc} = 2(\lambda - \lambda^{-2})c_1 + \frac{1 - \lambda^{-3}}{\sqrt{2\lambda + \lambda^{-2}}}c_2 + 2(3c_4 + 1)(\lambda^2 + 2\lambda^{-1})^{3c_4}(\lambda - \lambda^{-2})c_3. \tag{14}$$

Biaxial Extension Mode. The nominal stresses in two extension directions as a function of principal stretches in biaxial extension mode for incompressible isotropic hyperelastic materials are worked out as

$$P_{be1} = 2(\lambda_1 - \lambda_1^{-3}\lambda_2^{-2})\left[c_1 + (3c_4 + 1)(\lambda_1^2 + \lambda_2^2 + \lambda_1^{-2}\lambda_2^{-2})^{3c_4}c_3\right] + \frac{\lambda_1\lambda_2^2 - \lambda_1^{-3}}{\sqrt{\lambda_1^2\lambda_2^2 + \lambda_1^{-2} + \lambda_2^{-2}}}c_2, \tag{15}$$

$$P_{be2} = 2(\lambda_2 - \lambda_1^{-2}\lambda_2^{-3})\left[c_1 + (3c_4 + 1)(\lambda_1^2 + \lambda_2^2 + \lambda_1^{-2}\lambda_2^{-2})^{3c_4}c_3\right] + \frac{\lambda_1^2\lambda_2 - \lambda_2^{-3}}{\sqrt{\lambda_1^2\lambda_2^2 + \lambda_1^{-2} + \lambda_2^{-2}}}c_2. \tag{16}$$

Equibiaxial Extension Mode. The nominal stress as a function of principal stretch in equibiaxial extension mode for incompressible isotropic hyperelastic materials is simplified by substituting $\lambda_2 = \lambda_1 = \lambda$ into (15) or (16) and rearranging yields

$$P_{ee} = 2(\lambda - \lambda^{-5})c_1 + \frac{\lambda^3 - \lambda^{-3}}{\sqrt{\lambda^4 + 2\lambda^{-2}}}c_2 + 2(3c_4 + 1)(2\lambda^2 + \lambda^{-4})^{3c_4}(\lambda - \lambda^{-5})c_3. \tag{17}$$

Pure Shear Mode. The nominal stress as a function of principal stretch in pure shear mode for incompressible isotropic hyperelastic materials turns out to be

$$P_{ps} = 2(\lambda - \lambda^{-3})c_1 + \frac{\lambda - \lambda^{-3}}{\sqrt{\lambda^2 + \lambda^{-2} + 1}}c_2 + 2(3c_4 + 1)(\lambda^2 + \lambda^{-2} + 1)^{3c_4}(\lambda - \lambda^{-3})c_3. \tag{18}$$

Simple Shear Mode. The nominal shear stress as a function of shear stretch in simple shear mode for incompressible isotropic hyperelastic materials is given by

$$P_{ss} = 2\kappa c_1 + \frac{\kappa}{\sqrt{\kappa^2 + 3}}c_2 + 2(3c_4 + 1)\kappa(\kappa^2 + 3)^{3c_4}c_3. \tag{19}$$

Variables λ and κ in the CSE model are normal and shear stretches, respectively.

2.3 Uniaxial Constitutive Equation with Residual Stretch

The general CSE constitutive equation in uniaxial extension mode can be modified to capture cyclic mechanical responses with residual stretches as

$$P_{ur} = 2(\Lambda - \Lambda^{-2})c_1 + \frac{1 - \Lambda^{-3}}{\sqrt{2\Lambda + \Lambda^{-2}}}c_2 + 2(3c_4 + 1)(\Lambda^2 + 2\Lambda^{-1})^{3c_4}(\Lambda - \Lambda^{-2})c_3, \tag{20}$$

where the ratio of total stretch to residual stretch is also called the normalized stretch by a residual stretch, $\Lambda = \lambda/\lambda_r \in [1, \lambda_p/\lambda_r]$, in extension mode.

2.4 Stress-Softening Ratio

The Mullins effect refers to the stretch induced stress-softening for many materials. Stress-softening curves of the Mullins effect are commonly predicted by a damage or softening function. The softened stress at the nth circle, P_n, can be related to stress from virgin loading, P_0, at a certain pre-stretch, λ_p, by the following stress-softening ratio

$$R_{sn} = \frac{P_n(\lambda_p)}{P_0(\lambda_p)} = \left(1 + \frac{s_2}{n}\right)^{-(\lambda_p - 1)s_1 n}, \quad (n = 0, 1, 2, 3, \cdots), \tag{21}$$

where the two softening parameters, s_1 and s_2, for the stress-softening ratio, R_{sn}, are determined by experiments. Unlike common practices, the stress-softening ratio is only used to predict the softened stress points at untested pre-stretches rather than whole curves. Untested cyclic mechanical responses are embedded in the constitutive parameters fitted from experimental tests. Thus, interpolations of constitutive parameters are desired.

2.5 Interpolation of Constitutive Parameters

The general CSE functional or model will be used to fit the unloading and reloading experimental data at tested pre-stretches. For predictions of unloading and reloading curves at untested pre-stretches, the weighted piecewise two-point interpolation will be used

$$c_i(\Lambda_p) = (2 - w)\frac{\Lambda_p - \Lambda_{p2}}{\Lambda_{p1} - \Lambda_{p2}}c_i(\Lambda_{p1}) + w\frac{\Lambda_p - \Lambda_{p1}}{\Lambda_{p2} - \Lambda_{p1}}c_i(\Lambda_{p2}), \quad (i = 1, 2, 3, 4), \tag{22}$$

where a normalized untested pre-stretch, Λ_p, falls within the nearest neighborhood between the normalized tested pre-stretches Λ_{p1} and Λ_{p2}. For predictions of untested reloading curves, the four constitutive parameters will be interpolated in such a way that changing the weight $w \in (0, 2)$ until the difference between the fitted experimental stress-softening (21) and the CSE model predicted stress-softening with constitutive parameters interpolated by (22) at the normalized untested pre-stretch is numerically minimized. For predictions of untested unloading curves, the four constitutive parameters can be determined similarly but the stress on virgin loading curve at an untested pre-stretch will be targeted. In essence, the start and end points of an untested curve, along with tested curves, are used to simultaneously predict constitutive parameters at an untested pre-stretch normalized by residual stretch.

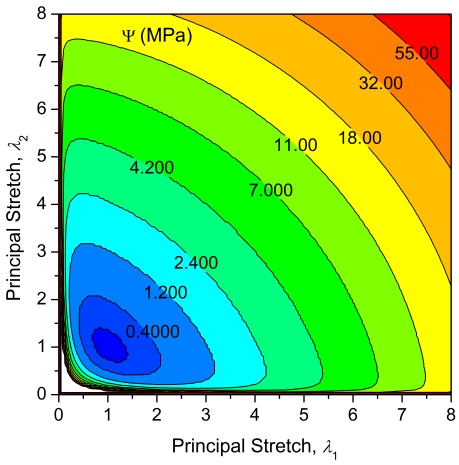

Figure 1. Contour of general CSE model for Treloar's uniaxial extension test.

Table 1. Constitutive parameters of CSE model for Treloar's uniaxial extension test.

Material	c_1(MPa)	c_2(MPa)	c_3(MPa)	c_4
NR-S8	0.1461648	0.0818923	3.7833917×10^{-7}	0.9828514

2.6 Residual-Stretch Ratio

For untested permanent stretch sets or residual stretches, λ_r, the piecewise three-point interpolation among tested residual stretches can be used. Considering the cyclic residual stretches, λ_{rn}, due to viscous heating effects, the residual-stretch ratio, R_{rn}, can be defined as

$$R_{rn} = \frac{\lambda_{rn}(\lambda_p)}{\lambda_{r0}(\lambda_p)} = 1 + (\lambda_p - 1)r_1 \ln(1+n), \quad (n = 0, 1, 2, 3, \cdots), \tag{23}$$

where the parameter, r_1, for the residual-stretch ratio is determined by experiments.

3 Applications of General CSE Model

3.1 Predictive Constitutive Modeling of Unfilled NR Rubber

The uniaxial extension, uniaxial compression, equibiaxial extension, biaxial extension, pure shear, and converted simple shear tests of an unfilled and vulcanized natural rubber with 8 phr sulfur (NR-S8) have been conducted at 20°C by Treloar [45]. The Treloar's experiments with all specimens taken from a single sheet of the material are usually used as a benchmark for evaluating constitutive models of incompressible isotropic hyperelastic materials [46,47,48]. The constitutive parameters of the general CSE constitutive equation in uniaxial extension mode (14) for Treloar's test data have numerically been solved by the trial-and-error-on-digit (TED) method and the linear least square (LLSQ) method combined by Zhao [49]. The contour of the general CSE functional is depicted in **Figure 1**. The constitutive parameters calibrated in uniaxial extension mode have been submitted into (14), (17), (15), (18), and (19) to predict tested but unfitted finite deformations in uniaxial compression, equibiaxial extension, biaxial extension, pure shear, and simple shear modes, respectively. The comparison between the Treloar's tests and the general CSE model is shown in **Figure 2**. The constitutive parameters fitted for Treloar's uniaxial extension test are listed in **Table 1**.

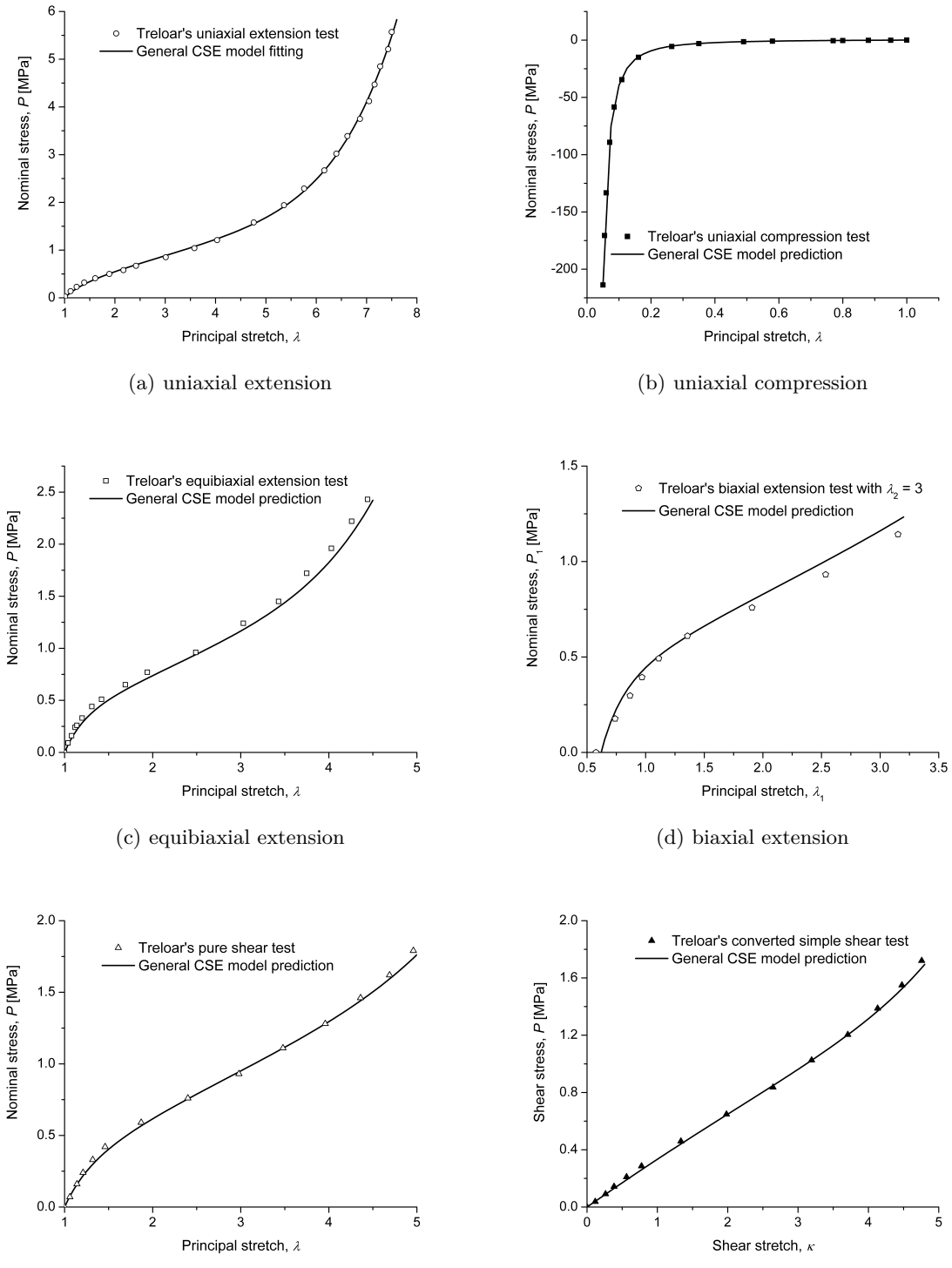

(a) uniaxial extension

(b) uniaxial compression

(c) equibiaxial extension

(d) biaxial extension

(e) pure shear

(f) simple shear

Figure 2. Comparison between Treloar's tests and general CSE model.

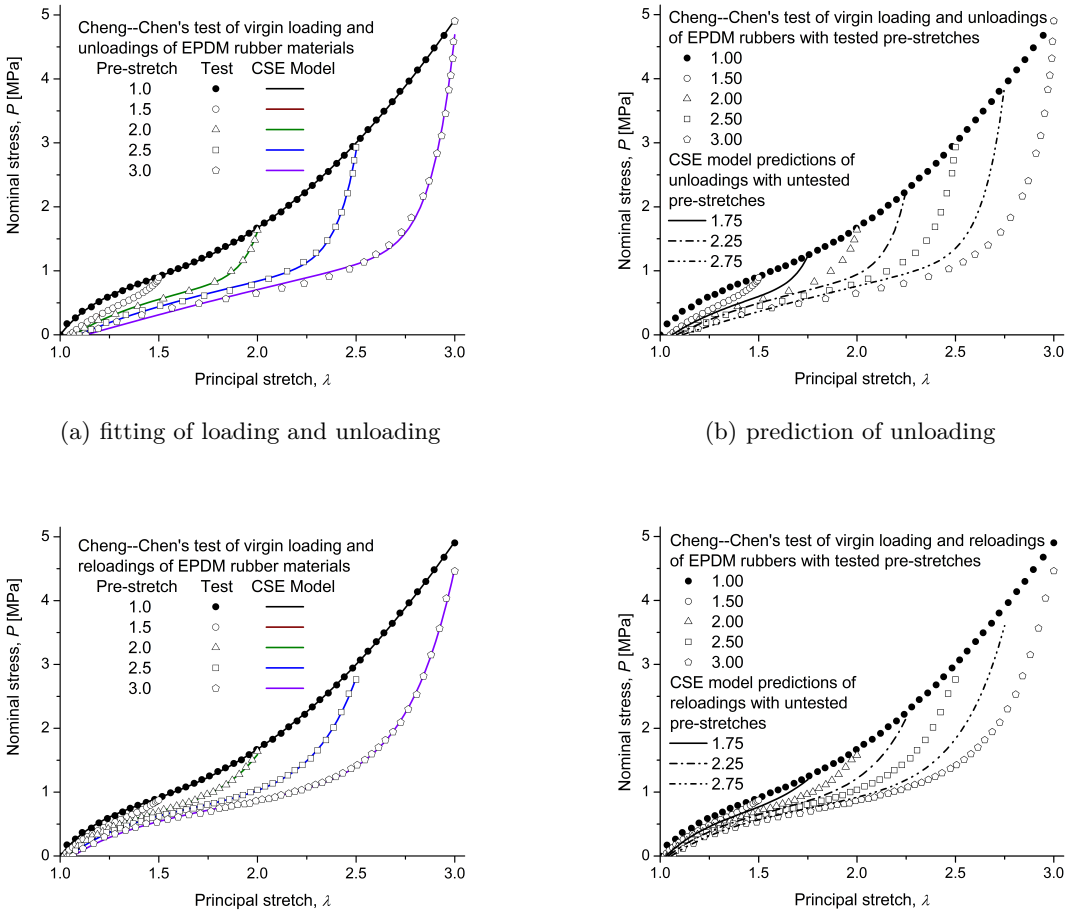

(a) fitting of loading and unloading

(b) prediction of unloading

(c) fitting of reloading

(d) prediction of reloading

Figure 3. Comparison between Cheng–Chen's test and general CSE model.

3.2 Predictive Constitutive Modeling of Filled EPDM Rubber

Cyclic uniaxial extension tests of filled ethylene-propylene-diene monomer (EPDM) rubbers have been conducted at room temperature with different stretch rates by Cheng and Chen [50]. The uniaxial extension test with the stretch rate of 0.004/s and the pre-stretches of 1.5, 2.0, 2.5, and 3.0, increasing every 3 cycles has been selected. A self-developed graphics digitizer with MATLAB has been used to read out all the related experimental data in the zeroth and first cycles. The constitutive parameters of the CSE constitutive equation (14) for tested virgin loading data and the CSE constitutive equation with residual stretches (20) for tested unloading and reloading data have respectively been solved by the TED-LLSQ method. The stress-softening data at untested pre-stretches of 1.75, 2.25, and 2.75 is predicted by the stress-softening ratio equation (21). The constitutive parameters of unloading and reloading with stress-softening curves at untested pre-stretches of 1.75, 2.25, and 2.75 are determined by the weighted two-point interpolation equation (22). The comparison between the Cheng–Chen's test and the general CSE model for virgin loading, unloading, and reloading responses is shown in **Figure 3**.

3.3 Predictive Constitutive Modeling of Filled SBR Rubber

The cyclic uniaxial extension test of styrene-butadiene rubbers (SBR) filled with carbon-black has been conducted at room temperature with the stretch rate of 0.001/s by Diani, Fayolle, and Gilormini [39].

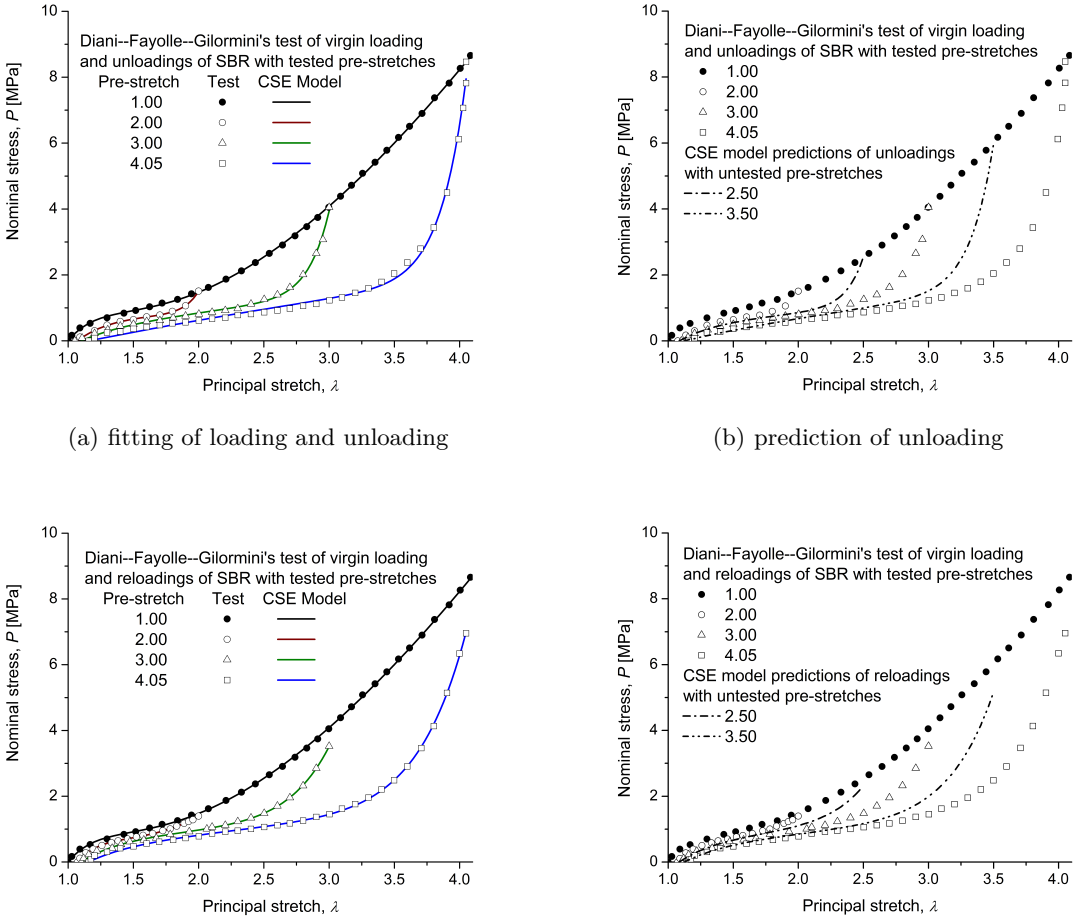

(a) fitting of loading and unloading

(b) prediction of unloading

(c) fitting of reloading

(d) prediction of reloading

Figure 4. Comparison between Diani–Fayolle–Gilormini's test and general CSE model.

The uniaxial extension test was performed with the pre-stretches of 2.00, 3.00, and 4.05, increasing every 5 cycles. A self-developed graphics digitizer with MATLAB has been used to read out all the related experimental data with the cycle numbers of $n = 0$ and $n = 1$. The constitutive parameters of the CSE constitutive equation (14) for tested virgin loading data ($n = 0$) and the CSE constitutive equation (20) for tested unloading and reloading data ($n = 1$) have respectively been solved by the TED-LLSQ method. The stress-softening data at untested pre-stretches of 2.5 and 3.5 is predicted by the stress-softening ratio equation (21). The constitutive parameters of unloading and reloading with stress-softening curves at untested pre-stretches of 2.5 and 3.5 are determined by the weighted piecewise two-point interpolation equation (22). The comparison between the Diani–Fayolle–Gilormini's test and the general CSE model of virgin loading, unloading, and reloading behaviors is shown in **Figure 4**.

4 Discussion

4.1 Predictive Constitutive Modeling of Unfilled Rubber

The convexity of a stored energy functional can be shown on a contour plot. For the contour plot of the general CSE functional (11), the constitutive parameters fitted from Treloar's uniaxial extension test are listed in **Table 1** and the three corresponding invariants, $I_1 = \lambda_1^2 + \lambda_2^2 + (\lambda_1\lambda_2)^{-2}$, $I_2 = \lambda_1^2\lambda_2^2 + \lambda_1^{-2} + \lambda_2^{-2}$,

and $I_3 = 1$, are used. As shown in **Figure 1**, the clamshell shaped contour lines radiate outwardly from the zero energy location with the coordinate of $(\lambda_1, \lambda_2) = (1, 1)$ and expand with the increase of stored energy values, indicating the convexity of the general CSE functional for Treloar's tests.

Many constitutive models can fit uniaxial extension tests. A constitutive model fitted or calibrated in uniaxial extension tests, however, could fail to predict responses of biaxial extension tests and tests in other deformation modes as emphasized by Marckmann and Verron [51]. Furthermore, constitutive parameters simultaneously calibrated in multiple deformation modes could pollute the overall accuracy since experimental tests at different deformation modes possess different accuracies, different amounts of deformations, and even different stabilities. Among which, uniaxial extension tests exhibit the best accuracy, the largest deformation range, and the greatest stability. Thus, in this predictive continuum constitutive modeling, the constitutive parameters fitted from Treloar's uniaxial extension test are used to predict tested but unfitted finite deformations in uniaxial compression, equibiaxial extension, biaxial extension, pure shear, and simple shear modes plotted in **Figure 2**. As shown, the predictions are accurate in all the selected deformation modes. The equibiaxial extension test and uniaxial compression test with the bubble inflation technique reduce the usual overestimation. With the assumption of incompressibility, superposition of a hydrostatic pressure to cancel the in-plane tensile stresses and to construct the out-of-plane compressive stress converts equibiaxial extension test data into uniaxial compression test data by Treloar [52] and the original uniaxial compression test data is given by Treloar [45]. The biaxial extension test data obtained by sequentially combining uniaxial extension and pure shear tests by Treloar are obtained from the article by Chagnon, Marckmann, and Verron [47]. The Treloar's simple shear test data is transformed from his pure shear test data. The equations, $\kappa = \lambda - \lambda^{-1}$ and $P_{ss} = P_{ps}/(1 + \lambda^{-2})$, are used for the transformation.

As listed in **Table 1**, the value of c_4 for Treloar's uniaxial extension test is close to but not equal to 1. Nevertheless, the general CSE model with variable c_4 indeed achieves better predictive constitutive modeling of Treloar's tests than those with a constant value, $c_4 = 1$, as initially studied by Zhao [43]. All in all, the general CSE model fits the uniaxial extension test and predicts unfitted finite deformations in the different deformation modes for Treloar's experimental tests, indicating the quality of the CSE functional as a predictive constitutive model of the unfilled rubber. Benefits of the general CSE model with variable c_4 will be further demonstrated in predictive constitutive modeling cyclic uniaxial extension responses of filled EPDM and SBR rubbers with the Mullins effect.

4.2 Predictive Constitutive Modeling of Filled Rubber

For filled rubbers under cyclic loading, the constitutive parameters of the CSE constitutive equation (20) are tacitly understood as variables due to damaging, softening, and other effects based on the method of variation of the constants. For residual stretches, the CSE constitutive equation (20) is augmented from (14) based on the multiplicative decomposition of the deformation gradient into elastic and plastic parts. With $\mathbf{F}_e = \mathbf{F}\mathbf{F}_p^{-1}$, related curve fitting, predicting, and finite element implementation can be treated as elastic deformations. Indeed, without unloading or reloading, it is difficult to differentiate a plastic deformation from total deformation and residual stretches are truly plastic deformations.

Predictive constitutive modeling cyclic responses of filled rubbers with the Mullins effect covers the virgin loading, first unloading, and first reloading experimental test at different pre-stretches with stress-softening and residual stretches. For the following cycles, the same method can be applied. By the same token, hysteresis loops can be fitted and predicted. The permanent stress set or residual stress can be readily handled by simple summation and subtraction operations. For the Mullins effect with anisotropy, transversely isotropic constitutive models are usually utilized, which is beyond the scope of this study.

By and large, the general CSE functional and its derived CSE constitutive equations, along with the stress-softening ratio, residual-stretch ratio, and the weighted piecewise two-point interpolation function, offer a new method for predictive constitutive modeling finite deformations and physical understanding deformation mechanisms of filled rubbers with the Mullins effect.

Table 2. Evolution of constitutive parameters for filled EPDM rubber by general CSE model.

λ_p	λ_r	c_1 (MPa)	c_2 (MPa)	c_3 (MPa)	c_4	Note
1.00	1.00000	−2.0736732	3.2081138	9.28779×10^{-01}	0.1140723	fit-loading
1.50	1.05083	0.2110987	0.7983706	3.53972×10^{-19}	9.9364224	fit-unloading
1.75	1.05948	0.2318063	0.4319945	5.88092×10^{-14}	6.2643379	predict-unloading
2.00	1.07000	0.2350243	0.3750591	6.79481×10^{-14}	5.6936905	fit-unloading
2.25	1.08250	0.2654665	0.0961702	4.55107×10^{-14}	5.3651124	predict-unloading
2.50	1.09667	0.2906265	−0.1343271	2.69666×10^{-14}	5.0935478	fit-unloading
2.75	1.11250	0.3122325	−0.4062492	1.29057×10^{-14}	4.9374487	predict-unloading
3.00	1.13000	0.3250858	−0.5680146	4.54099×10^{-15}	4.8445860	fit-unloading
1.50	1.02200	−27603.126	4.3105877	$2.75989\times10^{+4}$	0.0000208	fit-reloading
1.75	1.02838	0.0022600	1.6306945	1.34641×10^{-5}	1.8272009	predict-reloading
2.00	1.03475	0.0022656	1.6306945	7.86152×10^{-6}	1.8272009	fit-reloading
2.25	1.04054	0.1392870	0.9686405	6.46982×10^{-7}	2.1419788	predict-reloading
2.50	1.04633	0.1463470	0.9345284	2.75255×10^{-7}	2.1581976	fit-reloading
2.75	1.05598	0.1815272	0.6372036	1.02270×10^{-7}	2.2049422	predict-reloading
3.00	1.06564	0.1930051	0.5401984	4.58317×10^{-8}	2.2201931	fit-reloading

4.3 Analyses of Constitutive Parameters

The constitutive parameters for predictive constitutive modeling Cheng–Chen's test and Diani–Fayolle–Gilormini's test are listed in **Table 2** and **Table 3**, respectively.

The general CSE model, along with the stress-softening ratio, residual-stretch ratio, and the weighted piecewise two-point interpolation function, accurately fits and predicts finite deformations with the Mullins effect for both the Cheng–Chen's test shown in **Figure 3** and the Diani–Fayolle–Gilormini's test shown in **Figure 4**.

The accuracy of using a damage or softening function to predict entire mechanical responses of the Mullins effect is scanty. The relevance of continuum damage mechanics as applied to the Mullins effect has been addressed by Chagnon *et al.* [53]. One of the most crucial findings in this study is that not all constitutive parameters are decreasing or softening with increasing pre-stretch. The detailed evolution of constitutive parameters as a function of pre-stretches will be elaborated on to elucidate physical mechanisms of the Mullins effect.

Constitutive Parameter c_1. In the general CSE functional, the constitutive parameter c_1 describes the strength due to one-dimensional normal stretches. During the cyclic loading processes of both EPDM and SBR rubbers, c_1 changes from a negative value (damage), quickly to an even greater negative value (severe damage), then to zero, and a positive number, starting to increase its values (hardening instead of softening) as pre-stretch increases from 1 to its maximum value. This phenomenon is similar to muscle growth, in which short fibers are initially fractured by virgin stretching and long fibers grow as the stretching goes on, resulting in greater strength than before. In the two rubber cases, likewise, short bonds within crosslinks may be ruptured and more long bonds are rearranged to enhance the strength due to normal stretches. The short bond rapture mechanism was proposed by Bueche [54]. This physical mechanism has also been addressed by Marckmann *et al.* [31].

Constitutive Parameter c_2. The constitutive parameter c_2 represents the strength due to two-dimensional shear stretches. During the cyclic loading processes of both EPDM and SBR rubbers, c_2 decreases (with damaging in unloading) as pre-stretch increases from 1 to its maximum value. With

Table 3. Evolution of constitutive parameters for filled SBR rubber by general CSE Model.

λ_p	λ_r	c_1 (MPa)	c_2 (MPa)	c_3 (MPa)	c_4	Note
1.00	1.00000	−65.1887663	5.0222194	$6.28490\times10^{+01}$	0.0043110	fit-loading
2.00	1.07315	−0.0229894	1.9760616	1.43451×10^{-10}	4.1019102	fit-unloading
2.50	1.08411	0.1524263	0.8415104	5.65523×10^{-11}	3.6772231	predict-unloading
3.00	1.10129	0.2378517	0.2889966	1.42337×10^{-11}	3.4704052	fit-unloading
3.50	1.12467	0.2839642	−0.3720592	3.08712×10^{-12}	3.3954942	predict-unloading
4.05	1.15956	0.3071800	−0.5655930	1.76294×10^{-13}	3.5030108	fit-unloading
2.00	1.07315	−42397.495	6.2605695	$4.23935\times10^{+4}$	0.0000111	fit-reloading
2.50	1.08411	0.1326606	1.2041993	6.12219×10^{-6}	1.6467686	predict-reloading
3.00	1.10129	0.1326643	1.2041993	2.39156×10^{-6}	1.6467686	fit-reloading
3.50	1.12467	0.1845315	0.6871242	5.95312×10^{-7}	1.7211344	predict-reloading
4.05	1.15956	0.2057522	0.5702242	1.22098×10^{-7}	1.8061242	fit-reloading

the increase of pre-stretch, the strength of rubbers due to shear stretch decreases, making one part of the contribution for stress-softening. This phenomenon may correspond to the molecules slipping theory established by Houwink [55]. Based on atomic force microscopic observations, the short bond rupture and chain slippage were attributed to the origin of the Mullins effect by Clément, Bokobza, and Monnerie [56].

Constitutive Parameter c_3. The constitutive parameter c_3 captures the strength due to three-dimensional ellipsoidal deformations. During the cyclic loading processes of both EPDM and SBR rubbers, c_3 decreases as pre-stretch increases from 1 to its maximum value. With the increase of pre-stretch, the strength of rubbers due to ellipsoidal deformations decreases, making another part of the contribution for stress-softening. However, the contribution of c_3 term is also related to c_4. For the example of Cheng–Chen's uniaxial extension test of reloading curves at different pre-stretches, the values of c_3 decreases while that of c_4 increases as pre-stretch increases. The stress-softening contributed by both c_3 and c_4 for Cheng–Chen's uniaxial extension reloading test is depicted in **Figure 5**. A similar trend for Diani–Fayolle–Gilormini's reloading test has been observed. In the two filled rubber cases, the three-dimensional rubber-filler interface is weakened during stretching. This phenomenon may be explained by the fuzzy interface mechanism observed through the combination of small- and wide-angle X-ray scattering by Sui *et al.* [57]. The gradual loss of the physical crosslinks across the fuzzy interface region, due to gradual decreases of electron density and crosslink density, is believed to be the origin of the Mullins effect.

Constitutive Parameter c_4. The constitutive parameter c_4 delineates the degree of alignment for elastomeric chains. In the virgin loading cases, c_4 has values quite less than 1, indicating initial random alignment of elastomeric chains. In both EPDM and SBR rubbers, c_4 decreases during unloading cases as pre-stretch increase while c_4 increases during reloading cases. In the current predictive constitutive modeling, the first cycle of unloading and reloading has been studied.

4.4 Summary

Important findings from predictive constitutive modeling monotonic and cyclic mechanical responses of rubbers are summarized as follows:

– For Treloar's tests of the NR-S8 rubber, the general CSE model produces both accurate curve-fitting of uniaxial extension test and accurate predictions of uniaxial compression, equibiaxial extension, biaxial extension, pure shear, and simple shear tests. The general CSE model with variable c_4 becomes more versatile than the CSE model with the constant of $c_4 = 1$;

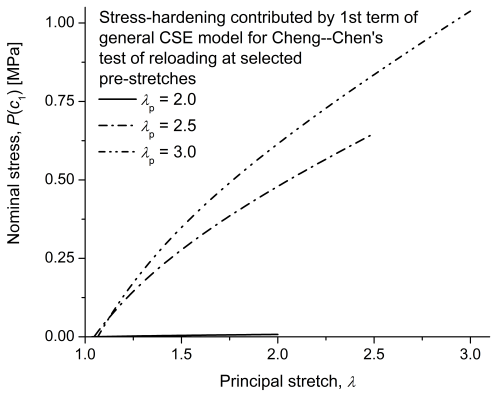

(a) stress-strengthening by c_1 term

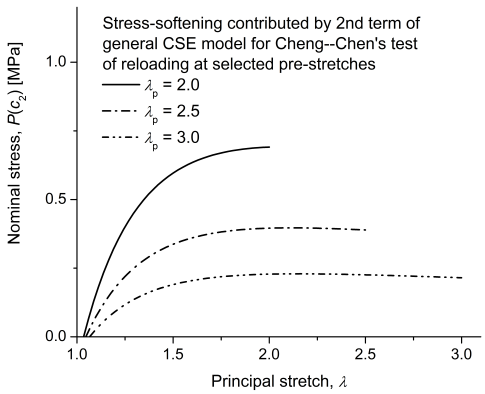

(b) stress-softening by c_2 term

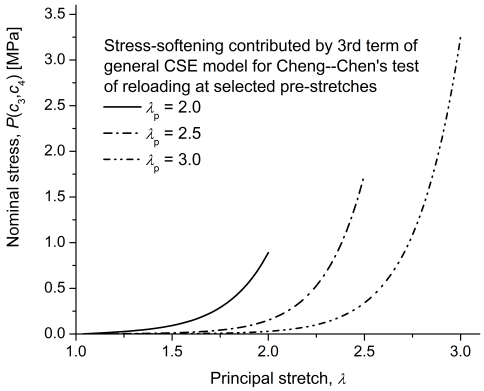

(c) stress-softening by c_3 term

Figure 5. Term-wised stress changes in general CSE model for Cheng–Chen's test.

- The general CSE model, along with the stress-softening ratio, residual-stretch ratio, and the weighted piecewise two-point interpolation function, offers a new method in predictive constitutive modeling of filled rubbers with the Mullins effect;
- As shown in **Figure 5**, the c_1 term increases stress while the c_2 or c_3 term decreases stress as pre-stretches increase in the general CSE model. Not all terms of the general CSE model soften the stress, making traditional predictions of the Mullins effect using a stress-softening function difficult to be accurate;
- In the new method, the start and end points of an untested curve, along with tested curves, are used to predict constitutive parameters for reloading or unloading responses at an untested pre-stretch;
- Multiple physical mechanisms result in the Mullins effect. Each physical mechanism dominates the stress-changing process at different pre-stretches.
- At small stretches, the values of c_1 are negative, causing damage due to short bond rupture. The stress due to normal stretches, however, is enhanced as pre-stretch increases as shown in **Figure 5**(a);
- At medium stretches, the c_2 term reaches its maximum value, dominating the stress-softening due to shear stretch or molecular-slipping as shown in **Figure 5**(b);
- At large stretches, the c_3 term dominates the stress-softening due to ellipsoidal deformation or interface-softening by loss of physical crosslinks as shown in **Figure 5**(c);

– Both damaging and softening effects occur during the cyclic uniaxial extension tests of EPDM and SBR rubbers with the Mullins effect.

5 Conclusions

For Treloar's tests of the unfilled NR-S8 rubber, the general CSE model calibrated in uniaxial extension test accurately predicts uniaxial compression, equibiaxial extension, biaxial extension, pure shear, and simple shear tests. The contour of the general CSE functional based on Treloar's uniaxial extension test demonstrates its convexity.

The general CSE model, the stress-softening ratio, the residual-stretch ratio, and the weighted piecewise two-point interpolation function offer a new method for predictive constitutive modeling of filled rubbers with the Mullins effect. For both the Cheng–Chen's uniaxial extension test of EPDM rubber and Diani–Fayolle–Gilormini's uniaxial extension test of SBR rubber, the general CSE model fits the tested virgin loading, first unloading, and first reloading curves at different pre-stretches with stress-softening and residual stretches. The start and end points of an untested curve, along with tested curves, are used to predict the untested response in reloading or unloading at an untested pre-stretch.

Not all constitutive parameters decrease with the increase of pre-stretches, making the applications of a single softening function's ability to predict entire responses of the Mullins effect questionable. Both damaging and softening effects occur during the cyclic uniaxial extension tests of filled rubbers with the Mullins effect. Multiple physical mechanisms rather than a single mechanism cause the Mullins effect. The Mullins effect is caused by a combination of short bond rupture at small normal deformations, molecular-slipping at medium shear deformations, and interface softening due to decreases of physical crosslinks at large ellipsoidal deformations.

Acknowledgments. The author is grateful to Mahmoud A. El-Sherif for his continued encouragement and earlier support in mechanical characterizations of optical fibers, modeling for plain weaving of optical fibers, and finite element analyses during the integration of optical fibers into textile fabrics.

He is thankful to his family Jianming and Jiesi Zhao for their support, encouragement, and assistance in many ways.

References

1. L. Mullins, "Effect of stretching on the properties of rubber," *Rubber Chemistry and Technology*, vol. 21, no. 2, pp. 281–300, 1948.
2. A. Dorfmann and R. W. Ogden, "A constitutive model for the Mullins effect with permanent set in particle-reinforced rubber," *International Journal of Solids and Structures*, vol. 41, no. 7, pp. 1855–1878, 2004.
3. L. Mullins and N. R. Tobin, "Theoretical model for the elastic behavior of filler-reinforced vulcanized rubbers," *Rubber Chemistry and Technology*, vol. 30, no. 2, pp. 555–571, 1957.
4. A. S. Wineman and K. R. Rajagopal, "On a constitutive theory for materials undergoing microstructural changes," *Archives of Mechanics*, vol. 42, no. 1, pp. 53–75, 1990.
5. A. S. Wineman and H. E. Huntley, "On a constitutive theory for materials undergoing microstructural changes," *International Journal of Solids and Structures*, vol. 31, no. 23, pp. 3295–3313, 1994.
6. M. A. Johnson and M. F. Beatty, "A constitutive equation for the Mullins effect in stress controlled extension experiments," *Continuum Mechanics and Thermodynamics*, vol. 5, no. 4, pp. 301–318, 1993.
7. M. F. Beatty and S. Krishnaswamy, "A theory of stress-softening in incompressible isotropic materials," *Journal of the Mechanics and Physics of Solids*, vol. 48, no. 9, pp. 1931–1965, 2000.
8. A. E. Zúñiga and M. F. Beatty, "A new phenomenological model for stress-softening in elastomers," *Zeitschrift für angewandte Mathematik und Physik*, vol. 53, no. 5, pp. 794–814, 2002.
9. H. J. Qi and M. C. Boyce, "Constitutive model for stretch-induced softening of the stress–stretch behavior of elastomeric materials," *Journal of the Mechanics and Physics of Solids*, vol. 52, no. 4, pp. 2187–2205, 2004.
10. M. E. Gurtin and E. C. Francis, "Simple rate-independent model for damage," *Journal of Spacecraft*, vol. 18, no. 3, pp. 285–286, 1981.
11. J. C. Simo, "On a fully three-dimensional finite-strain viscoelastic damage model: formulation and computational aspects," *Computer Methods in Applied Mechanics and Engineering*, vol. 60, no. 2, pp. 153–173, 1987.

12. S. Govindjee and J. C. Simo, "A micro-mechanically based continuum damage model for carbon black-filled rubbers incorporating Mullins' effect," *Journal of the Mechanics and Physics of Solids*, vol. 39, no. 1, pp. 87–112, 1991.
13. ——, "Mullins effect and the strain amplitude dependence of the storage modulus," *International Journal of Solids and Structures*, vol. 29, no. 14-15, pp. 1737–1751, 1992.
14. E. A. De Souza Neto, D. Perić, and D. R. J. Owen, "A phenomenological three-dimensional rate-independent continuum damage model for highly filled polymers: formulation and computational aspects," *Journal of the Mechanics and Physics of Solids*, vol. 42, no. 10, pp. 1533–1550, 1994.
15. C. Miehe, "Discontinuous and continuous damage evolution in Ogden-type large-strain elastic materials," *European Journal of Mechanics A/Solids*, vol. 14, no. 5, pp. 697–720, 1995.
16. C. Miehe and J. Keck, "Superimposed finite elastic-viscoelastic-plastoelastic stress response with damage in filled rubbery polymers. Experiments, modelling and algorithmic implementation," *Journal of the Mechanics and Physics of Solids*, vol. 48, no. 2, pp. 323–365, 2000.
17. M. Klüppel and J. Schramm, "A generalized tube model of rubber elasticity and stress softening of filler reinforced elastomer systems," *Macromolecular Theory and Simulations*, vol. 9, no. 9, pp. 742–754, 2000.
18. H. Lorenz and M. Klüppel, "Microstructure-based modelling of arbitrary deformation histories of filler-reinforced elastomers," *Journal of the Mechanics and Physics of Solids*, vol. 60, no. 11, pp. 1842–1861, 2012.
19. R. Raghunath, D. Juhre, and M. Klüppel, "A physically motivated model for filled elastomers including strain rate and amplitude dependency in finite viscoelasticity," *International Journal of Plasticity*, vol. 78, pp. 223–241, 2016.
20. J. Plagge and M. Klüppel, "A physically based model of stress softening and hysteresis of filled rubber including rate- and temperature dependency," *International Journal of Plasticity*, vol. 89, pp. 173–196, 2017.
21. R. Dargazany and M. Itskov, "A network evolution model for the anisotropic mullins effect in carbon black filled rubbers," *International Journal of Solids and Structures*, vol. 46, no. 3, pp. 2967–2977, 2009.
22. ——, "Constitutive modeling of Mullins effect and cyclic stress softening in filled elastomers," *Physical Review E*, vol. 88, no. 1, pp. 012 602(1–24), 2013.
23. R. Dargazany, V. N. Khiêm, and M. Itskov, "A generalized network decomposition model for the quasi-static inelastic behavior of filled elastomers," *International Journal of Plasticity*, vol. 63, no. 12, pp. 94–109, 2014.
24. V. N. Khiêm and M. Itskov, "An averaging based tube model for deformation induced anisotropic stress softening of filled elastomers," *International Journal of Plasticity*, vol. 90, no. 12, pp. 96–115, 2017.
25. ——, "Analytical network-averaging of the tube model: Mechanically induced chemiluminescence in elastomers," *International Journal of Plasticity*, vol. 102, no. 11, pp. 1–15, 2018.
26. R. W. Ogden and D. G. Roxburgh, "A pseudo-elastic model for the Mullins effect in filled rubber," *Proceedings of Royal Society London A*, vol. 455, no. 1988, pp. 2861–2877, 1999.
27. A. Dorfmann and R. W. Ogden, "A pseudo-elastic model for loading, partial unloading and reloading of particle-reinforced rubber," *International Journal of Solids and Structures*, vol. 40, no. 11, pp. 2699–2714, 2003.
28. S. R. Rickaby and N. H. Scott, "A cyclic stress softening model for the Mullins effect," *International Journal of Solids and Structures*, vol. 50, no. 1, pp. 111–120, 2013.
29. C. Naumann and J. Ihlemann, "On the thermodynamics of pseudo-elastic material models which reproduce the Mullins effect," *International Journal of Solids and Structures*, vol. 69-70, pp. 360–369, 2015.
30. E. Septanika and L. Ernst, "Application of the network alteration theory for modeling the time-dependent behavior of rubber. Part I. General theory," *Mechanics of Materials*, vol. 30, no. 4, pp. 253–263, 1998.
31. G. Marckmann, E. Verron, L. Gornet, G. Chagnon, P. Charrier, and P. Fort, "A theory of network alteration for the mullins effect," *Journal of the Mechanics and Physics of Solids*, vol. 50, no. 9, pp. 2011–2028, 2002.
32. J. Diani, M. Brieu, and J. M. Vacherand, "A damage directional constitutive model for Mullins effect with permanent set and induced anisotropy," *European Journal of Mechanics A/Solids*, vol. 25, no. 3, pp. 483–496, 2006.
33. X. Zhao, "A theory for large deformation and damage of interpenetrating polymer networks," *Journal of the Mechanics and Physics of Solids*, vol. 60, no. 2, pp. 319–332, 2012.
34. Q. Wang and Z. Gao, "A constitutive model of nanocomposite hydrogels with nanoparticle crosslinkers," *Journal of the Mechanics and Physics of Solids*, vol. 94, pp. 127–147, 2016.
35. P. Zhu and Z. Zhong, "Modelling the mechanical behaviors of double-network hydrogels," *International Journal of Solids and Structures*, vol. 193-194, pp. 492–501, 2020.
36. ——, "Development of the network alteration theory for the Mullins softening of double-network hydrogels," *Mechanics of Materials*, vol. 152, pp. 103 658(1–7), 2021.
37. S. Cantournet, R. Desmorat, and J. Besson, "Mullins effect and cyclic stress softening of filled elastomers by internal sliding and friction thermodynamics model," *International Journal of Solids and Structures*, vol. 46, no. 11-12, pp. 2255–2264, 2009.

38. L. Mullins, "Softening of rubber by deformation," *Rubber Chemistry and Technology*, vol. 42, no. 1, pp. 339–362, 1969.
39. J. Diani, B. Fayolle, and P. Gilormini, "A review on the Mullins effect," *European Polymer Journal*, vol. 45, no. 3, pp. 601–612, 2009.
40. R. Diaz, J. Diani, and P. Gilormini, "Physical interpretation of the Mullins softening in a carbon-black filled SBR," *European Polymer Journal*, vol. 55, no. 19, pp. 4942–4947, 2014.
41. T. A. Vilgis, G. Heinrich, and M. Klüppel, *Reinforcement of polymer nano-composites: theory, experiments and applications*, 1st ed. Cambridge: Cambridge University Press, 2009.
42. R. S. Rivlin, "Large elastic deformations of isotropic materials IV. Further developments of the general theory," *Philosophical Transactions of the Royal Society A*, vol. 241, pp. 379–397, 1948.
43. F. Zhao, "Continuum constitutive modeling for isotropic hyperelastic materials," *Advances in Pure Mathematics*, vol. 6, no. 9, pp. 571–582, 2016.
44. ——, "Modeling and implementing compressible isotropic finite deformation without the isochoric–volumetric split," *Journal of Advances in Applied Mathematics*, vol. 5, no. 2, pp. 57–70, 2020.
45. L. R. G. Treloar, "Stress-strain data for vulcanised rubber under various types of deformation," *Transactions of the Faraday Society*, vol. 40, pp. 59–70, 1944.
46. M. C. Boyce and E. M. Arruda, "Constitutive models of rubber elasticity: A review," *Rubber Chemistry and Technology*, vol. 73, no. 3, pp. 504–523, 2000.
47. G. Chagnon, G. Marckmann, and E. Verron, "A comparison of the Hart-Smith model with Arruda-Boyce and Gent formulations for rubber elasticity," *Rubber Chemistry and Technology*, vol. 77, no. 4, pp. 724–735, 2004.
48. P. Steinmann, M. Hossain, and G. Possart, "Hyperelastic models for rubber-like materials: Consistent tangent operators and suitability for Treloar's data," *Archive for Applied Mechanics*, vol. 82, no. 9, pp. 1183–1217, 2012.
49. F. Zhao, "On constitutive modeling of arteries," *Journal of Advances in Applied Mathematics*, vol. 4, no. 2, pp. 54–68, 2019.
50. M. Cheng and W. Chen, "Experimental investigation of the stress-stretch behavior of EPDM rubber with loading rate effects," *International Journal of Solids and Structures*, vol. 40, no. 18, pp. 4749–4768, 2003.
51. G. Marckmann and E. Verron, "Comparison of hyperelastic models for rubberlike materials," *Rubber Chemistry and Technology*, vol. 79, no. 5, pp. 835–858, 2006.
52. L. R. G. Treloar, *The Physics of Rubber Elasticity*, 3rd ed. New York: Oxford University Press, 2005.
53. G. Chagnon, E. Verron, L. Gornet, G. Marckmann, and P. Charrier, "On the relevance of continuum damage mechanics as applied to the Mullins effect in elastomers," *Journal of the Mechanics and Physics of Solids*, vol. 52, no. 7, pp. 1627–1650, 2004.
54. F. Bueche, "Molecular basis for the Mullins effect," *Journal of Applied Polymer Science*, vol. 4, no. 10, pp. 107–114, 1960.
55. R. Houwink, "Slipping of molecules during the deformation of reinforced rubber," *Rubber Chemistry and Technology*, vol. 29, no. 3, pp. 888–893, 1956.
56. F. Clément, L. Bokobza, and L. Monnerie, "On the Mullins effect in silica filled polydimethylsiloxane networks," *Rubber Chemistry and Technology*, vol. 74, no. 5, pp. 846–870, 2001.
57. T. Sui, E. Salvati, S. Ying, G. Sun, I. P. Dolbnya, K. Dragnevski, C. Prisacariu, and A. M. Korsunsky, "Strain softening of nano-scale fuzzy interfaces causes Mullins effect in thermoplastic polyurethane," *Scientific Reports*, vol. 7, pp. 916 (1–9), 2017.

